European Journal of Radiology 181 (2024) 111808

Contents lists available at ScienceDirect

European Journal of Radiology

journal homepage: www.elsevier.com/locate/ejrad

# Impact of *deep Learning-enhanced contrast* on diagnostic accuracy in stroke CT angiography

Sebastian Steinmetz [a], Mario Alberto Abello Mercado [a], Sebastian Altmann [a], Antoine Sanner [b], Andrea Kronfeld [a], Marius Frenzel [a], Dongok Kim [c], Sergiu Groppa [d], Timo Uphaus [d], Marc A. Brockmann [a], Ahmed E. Othman [a,*]

[a] *Department of Neuroradiology, University Medical Center Mainz, Johannes Gutenberg University, Langenbeckstr. 1, 55131 Mainz, Germany*
[b] *Technical University of Darmstadt, Karolinenpl. 5, 64289 Darmstadt, Germany*
[c] *Department of Applied Bioengineering, Graduate School of Convergence Science and Technology, Seoul, Republic of Korea*
[d] *Department of Neurology, University Medical Center Mainz, Johannes Gutenberg University, Langenbeckstr. 1, 55131 Mainz, Germany*

ARTICLE INFO

*Keywords:*
Computed tomography angiography
Deep learning-augmented contrast enhancement
Denoising
Stroke
Vessel occlusion
Diagnostic accuracy

ABSTRACT

*Purpose:* To examine the impact of deep learning-augmented contrast enhancement on image quality and diagnostic accuracy of poorly contrasted CT angiography in patients with suspected stroke.

*Methods:* This retrospective single-centre study included 102 consecutive patients who underwent CT imaging for suspected stroke between 01/2021 and 12/2022, including whole brain volume perfusion CT (VPCT) and, specifically, a poorly contrasted CT angiography (defined as < 350HU in the proximal MCA). CT angiography imaging data was reconstructed using i.) an iterative reconstruction kernel (conventional CTA, c-CTA) as well as ii.) an iodine-based contrast boosting deep learning model (Deep Learning-enhanced CTA, DLe-CTA). For quantitative analysis, the slope, contrast-to-noise ratio (CNR), and signal-to-noise ratio (SNR) were determined. Qualitative image analysis was conducted by three readers, rating image quality and vessel-specific parameters on a 4-point Likert scale. Readers evaluated both datasets for cerebral vessel occlusion presence. VPCT served as the reference standard for calculating sensitivity and specificity.

*Results:* 102 patients were evaluated (mean age 69 ± 13 years; 70 men). DLe-CTA outperformed c-CTA in quantitative (all items $p < 0.001$) and qualitative image analysis (all items $p < 0.05$). VPCT revealed 58/102 patients with vascular occlusion. DLe-CTA resulted in significantly higher sensitivity compared to c-CTA ($p < 0.001$); (all readers put together: c-CTA: 142/174 [81.6 %; 95 % CI: 75.0 %-87.1 %] vs. DLe-CTA 163/174 [94 %; 95 % CI: 89.0 %-96.8 %]). One false positive finding occurred on DLe-CTA (specificity 1/132) [99.2 %; 95 % CI: 95.9 %-100 %].

*Conclusions:* Deep learning-augmented contrast enhancement improves the image quality and increases the sensitivity of detection vessel occlusions in poorly contrasted CTA.

## 1. Introduction

Stroke is a devastating medical condition and the second leading cause of death among the top five causes of cardiovascular-related deaths, with an increase of 47 % from 1990 (approximately 5 million deaths) to 2021 (approximately 7.4 million deaths) [1]. Computed tomography (CT) imaging, in particular CT angiography (CTA), plays a central role in assessing stroke patients by providing essential information about cerebral vessel occlusion and guiding therapeutic interventions [2].

One of the major challenges in CTA imaging arises from poor contrast images, in which interpreting physicians may miss vascular pathologies. There are few options besides repeating the scan for poorly contrasted CTA. If dual-energy CT is utilized, one may reconstruct monoenergetic images, called virtual monoenergetic imaging (VMI), enabling enhanced iodine contrast [3]. Furthermore, studies utilizing virtual monoenergetic imaging have shown the potential to improve the image quality of thoracic CT examinations and have led to improved

* Corresponding author at: Department of Neuroradiology, University Medical Center Mainz, Johannes Gutenberg University, Langenbeckst. 1, 55131 Mainz, Germany.
*E-mail addresses:* marius.frenzel@unimedizin-mainz.de (M. Frenzel), ahmed.e.othman@googlemail.com (A.E. Othman).

https://doi.org/10.1016/j.ejrad.2024.111808
Received 27 July 2024; Received in revised form 15 October 2024; Accepted 27 October 2024
Available online 28 October 2024

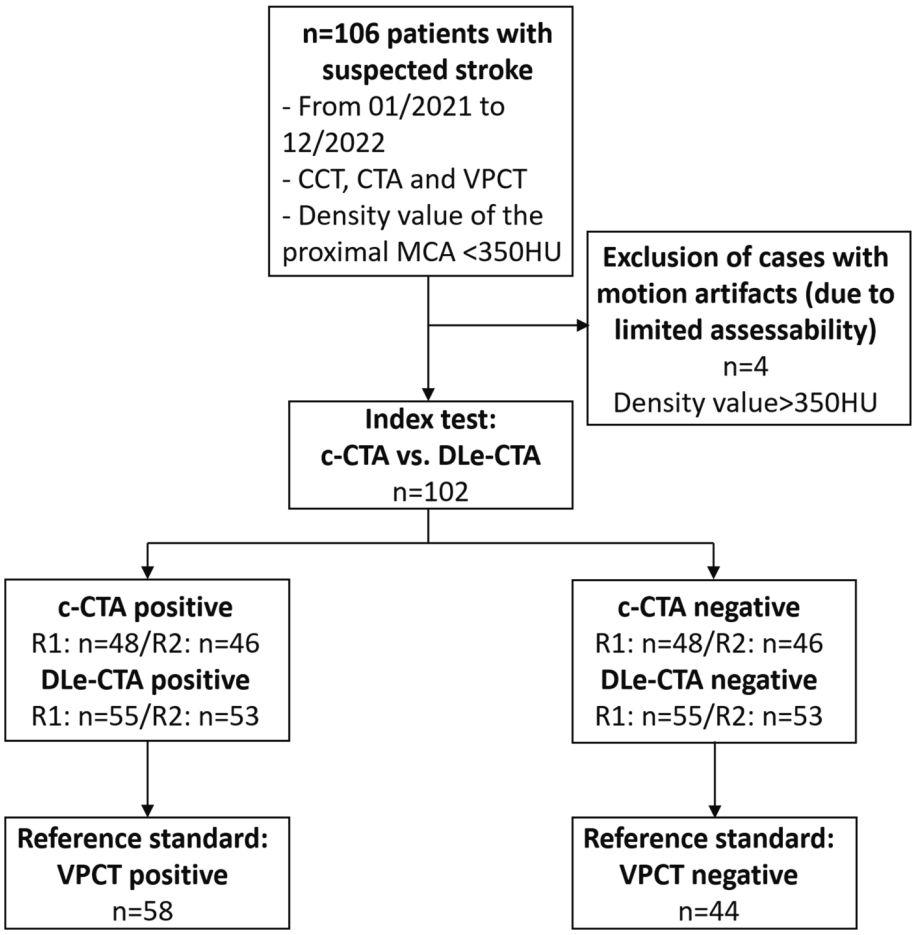


**Fig. 1.** Flowchart illustrating the study enrollment criteria. MCA = middle cerebral artery. c-CTA = conventional CTA. DLe-CTA = Deep Learning-enhanced CTA. R1-3 = Reader 1–3. VPCT = volume perfusion CT.

visualization of the vessels, among other structures, due to increased contrast intensity [4,5].

This study focuses on a deep learning model trained with dual-energy CT data to detect and enhance iodine-based contrast on single-spectrum CT scans. In addition, the image quality is improved by denoising. This shall improve the differentiation of the vessels from the brain parenchyma surrounding them. A big advantage is that the benefits of spectral imaging can be used device independent [6,7].

We hypothesized that this model may improve diagnostic accuracy for detecting cerebral vessel occlusions in patients with acute stroke. Therefore, this study aimed to assess the effects of deep learning-augmented contrast enhancement on image quality and diagnostic performance in poorly contrasted CTA.

## 2. Materials and methods

### 2.1. Study sample

This retrospective, single-centre study received approval from the local Ethics Committee, and all methods were performed in accordance with the 2008 version of the Declaration of Helsinki and were approved with a waiver for patient consent. We retrospectively identified consecutive patients with suspected ischemic stroke between 01/2021 and 12/2022 who underwent comprehensive CT imaging, including CCT, VPCT, and cerebral CTA. Inclusion criteria comprised poorly contrasted CTA, defined as a contrast density of less than 350 HU in the proximal M1 segment of the MCA.

An independent reader (S.A. with respectively 8 years of experience in neuro-imaging) evaluated all patients with fully recorded stroke protocol between 01/2021 and 12/2022 using the Sectra software (Sectra Workstation; Linköping, Sweden) to measure the contrast intensity manually.

Exclusion criteria were motion and metal artifacts that limited assessability as well as patients with incomplete stroke protocol with, for example, missing VPCT.

The cohort's identification and inclusion and exclusion criteria are given in a STARD flowchart (Fig. 1).

### 2.2. Stroke imaging protocol

The stroke imaging protocol included CCT, VPCT, and CTA. Images were acquired using an Aquilion Precision CT scanner (Canon Medical Systems Corporation; Japan). The scanner features a beam collimation of 0.25 mm x 160 rows.

### 2.3. Cranial Computed tomography

CCT was performed with 120 kV tube voltage, 0.5 mm collimation, and a 1.0-second rotation time. The axial CCT source images with a slice thickness of 0.5 mm were reconstructed in three planes with slice thicknesses of 3.0 mm in a 512 x 512 matrix.

### 2.4. Whole brain volume perfusion Computed tomography

Two sections at the level of the basal ganglia were imaged. The following scan parameters were used: z-axis, 8 cm; tube voltage, 80 kV;

rotation time, 0.35 s; scanning delay, 3.0 s; total scanning time, 59.2 s; acquisition intervals, 3.7 s.

To acquire cerebral perfusion data, we employed a commercially available Perfusion CT software (Canon Medical Systems Corporation), enabling the computation of cerebral blood flow, cerebral blood volume, mean transit time, and time-to-peak maps. Details of the contrast agent application are provided in the supplemental material (S1).

### 2.5. Computed tomography angiography

The CTA protocol comprised a tube voltage of 120 kV, a field of view of 180 mm, a rotation time of 0.35 s per rotation, and a pitch of 0.569. An adaptive iterative three-dimensional dose reduction tool (AIDR 3D; Canon Medical Systems Corporation) was applied. The axial CTA source images were reconstructed in three planes with slice thicknesses of 0.25 mm, 1.0 mm, and 3.0 mm, employing a reconstruction matrix of 1024 x 1024. Canon Medical Systems Corporation implemented an iterative reconstruction algorithm, the adaptive iterative three-dimensional dose reduction tool, which utilized an ultra-high-resolution adapted FC41 soft tissue Kernel (Conventional CTA, c-CTA). Details of the contrast agent application are provided in the supplemental material (S2).

### 2.6. Deep learning-based iodine contrast enhancement

All CTA DICOM datasets were additionally processed using a vendor-agnostic solution (ClariACE, ClariPi, Seoul, South Korea). It allows deep learning-based selective boosting of iodine contrast agent components in monoenergetic CT images (Deep Learning-enhanced CTA, DLe-CTA).

The vendor-agnostic program was developed as a contrast augmentation algorithm for low-contrast-dose CE CT using a deep learning model with a two-stage U-net architecture, trained on a dual-energy CT-derived dataset. For the training, varying degrees of synthetic low-contrast-dose contrast-enhanced CT images were generated by combining the virtual non-contrast component image with a weight-adjusted iodine component image of dual-energy CT, with weights ranging from 0.5 to 1.5. The first stage of U-net was a pre-trained network for image denoising that had been developed and validated previously (ClariCT.AI; ClariPi). The second stage of U-net was trained to accept a synthetic low-contrast-enhanced CT image and predict the weight-adjusted iodine component image. Subsequently, the model outputs the contrast-augmented image by scaling the pixel intensities of the predicted iodine component image with a user-defined boosting strength and then adding the intensity-scaled image back to the input image. The program also allows the user to specify the denoising strength for the denoising process.

Figure S1 provides an overview of the steps listed above.

**Table 1**
Patients characteristics.

| Parameter | All Patients (n = 102) |
|---|---|
| Age (y), mean, range | 68.6 (34–91) |
| Gender | 32 women |
| NIHSS | |
| Before therapy, median, range | 6.0 (1–30) |
| End of treatment, median, range | 2.5 (0–28) |
| mRS | |
| Before therapy, median, range | 3.0 (1–5) |
| End of treatment, median, range | 1.5 (0–5) |
| Mechanical thrombectomy (n, %) | 27 (26 %) |
| Intravenous lysis (n, %) | 33 (32 %) |
| Risk factors (n, %) | |
| High blood pressure | 75 (74 %) |
| Diabetes | 27 (26 %) |
| High blood cholesterol | 38 (37 %) |
| Nicotine abuse | 27 (26 %) |

Note.—y = years. NIHSS = National Institutes of Health Stroke Scale. mRS = Modified Ranking Scale.

### 2.7. Image presentation

The images were evaluated using the Sectra software (Sectra Workstation; Linköping, Sweden). The platform provides key features, including 3D volume rendering and maximum intensity projections with manually adjustable slice thickness.

### 2.8. Quantitative evaluation

The slope, contrast-to-noise ratio (CNR), and signal-to-noise ratio (SNR) were determined using a Matlab tool (S3).

### 2.9. Qualitative evaluation and detection of cerebral vessel occlusions

To evaluate the image quality of c-CTA and DLe-CTA, three readers (S.S., A.E.O., M.A.A.M. with respectively 3, 11, and 8 years of experience in neuro-imaging. S.S. had mainly general radiological experience as a young professional. In contrast, A.E.O. and M.A.A.M. are experts in the field of neuro-imaging.), blinded to clinical patient information and the type of reconstruction assessed various parameters using a 4-point Likert scale, with 4 representing the best (Table S1). The parameters included overall image quality, vessel contrast, artifacts, diagnostic confidence, image noise, and the assessability of proximal, intermediate, and subcortical vessels. The evaluation of the vessel-specific items was based on the cerebral vascular score of Ucar et al. [8].

An independent reader (S.A. with respectively 8 years of experience in neuro-imaging) evaluated VPCT, serving as the reference standard, for the presence of relevant perfusion deficit. The other readers assessed c-CTA and DLe-CTA for the presence of cerebral vessel occlusions. When calculating sensitivity and specificity, the total number of intracranial vascular occlusions was considered. A division into subgroups was carried out for a more detailed analysis. A distinction was made between proximal large vessel occlusions (PLVO; intracranial internal carotid artery (ICA), M1 segment of the MCA, the vertebral, and basilar artery), medium vessel occlusions (MeVO; MCA-M2, ACA-A1, PCA-P1 depending on their calibre-distal large or distal medium vessel occlusions, caliber 1 mm to 3 mm, NIHSS $\geq$ 5) and distal, medium vessel occlusions (DMVO; M3-M4, A2-A5, P2-P5, posterior inferior cerebellar artery, anterior inferior cerebellar artery, and superior cerebellar artery) [9,10].

To minimize recall bias, all reconstructions were independently evaluated during distinct sessions over a 6-week interval and presented to the readers in a randomized order. The individual readers conducted their assessments independently.

### 2.10. Statistics

Statistical analysis was performed using R-Stastistics (Version 4.1.3, R Foundation). First, we checked the data for normal distributions and determined the appropriate variable presentation. Continuous variables are given as mean ± 2 standard deviation if normally distributed and as median/IQR in case of a non-normal distribution.

The data for the quantitative analysis were assessed for normal distribution using the Shapiro-Wilk test. The mean and standard deviation of the items rated on the Likert scale – overall image quality, vessel contrast, artefacts, diagnostic accuracy, image noise and assessability of proximal, intermediate and subcortical vessels – were calculated, and statistical analysis was performed using the Wilcoxon signed-rank test. Regarding the Likert scale, scores 2, 3, and 4 indicate good quality, while a score of 1 indicates poor quality. Ordinal variables were compared by analyzing the distribution of Likert-scale values and calculating odds ratios (OR). For interrrater agreement, the multi-rater Fleiss' Kappa ($\chi$) was used. The level of agreement was defined as poor, $\chi < 0.21$; fair, $\chi =$ 0.21–0.40; moderate, $\chi = 0.41$–0.60; substantial, $\chi = 0.61$–0.80; and almost perfect, $\chi = 0.81$–1.0 [11].

VPCT was utilized to determine the presence or absence of cerebral

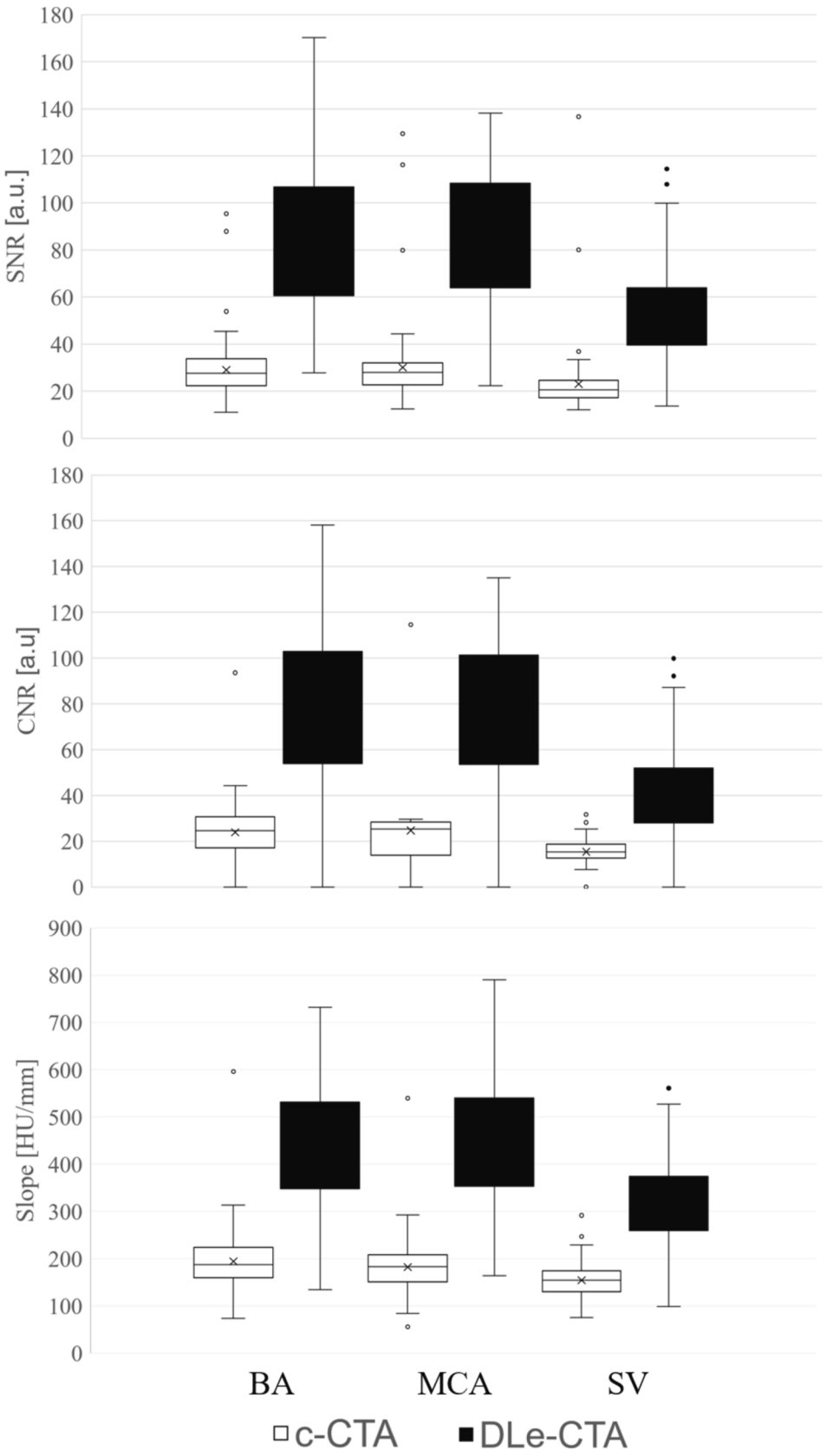


**Fig. 2.** Comparison of SNR, CNR and slope with c-CTA and DLe-CTA in BA, MCA and SV. SNR = signal to noise ratio. CNR = contrast to noise ratio. BA = basilar artery. MCA = middle cerebral artery. SV = subcortical vessel. c-CTA = conventional CTA. DLe-CTA = Deep Learning-enhanced CTA.

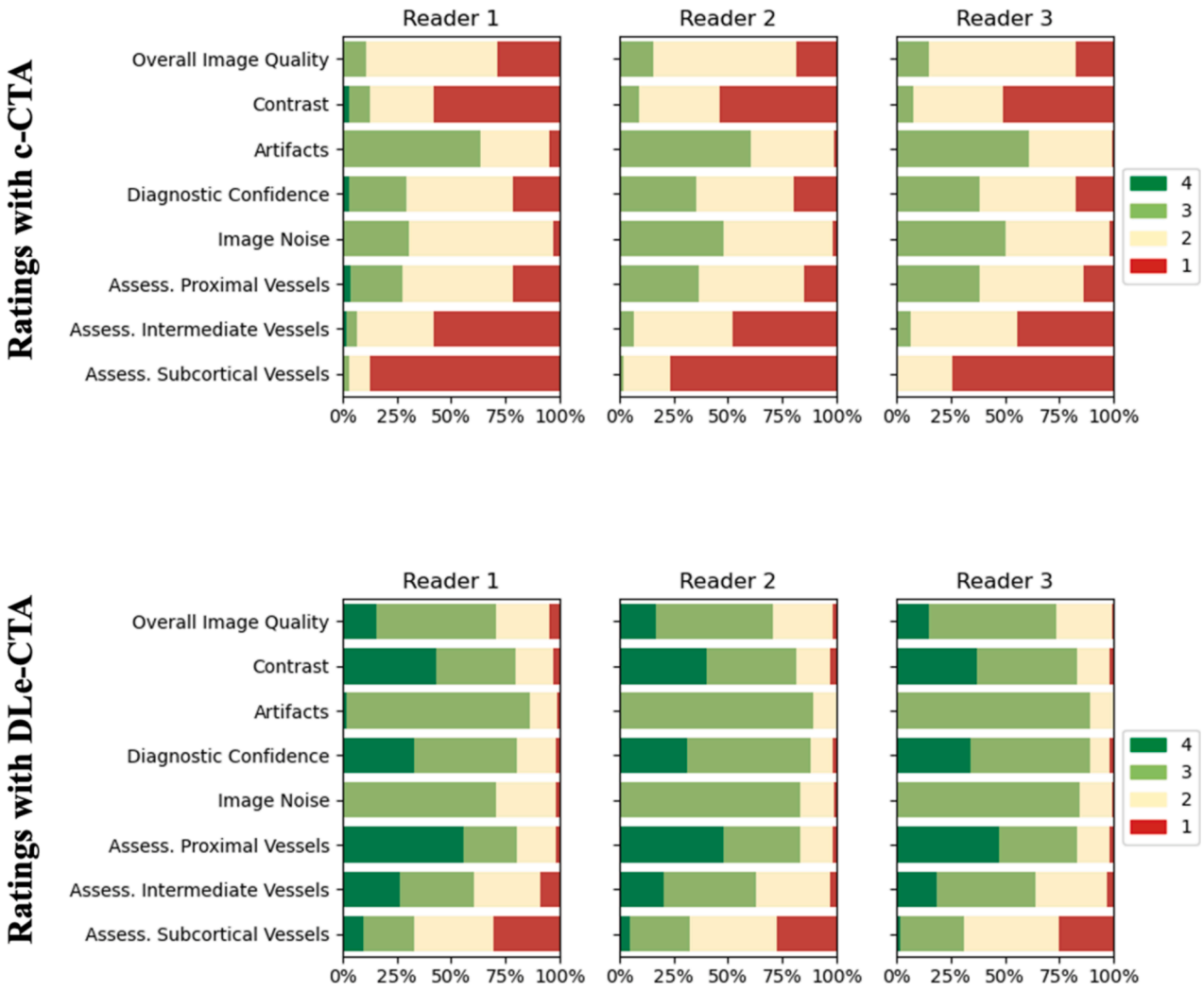


**Fig. 3.** Distribution of Likert scale values with 1 representing the worst and 4 the best. c-CTA = conventional CTA. DLe-CTA = Deep Learning-enhanced CTA.

vessel occlusions. Sensitivity and specificity, along with their 95 % Confidence Intervals (95 % CI), are reported for each reader and compared using McNemar's test.

P-values less than 0.05 were considered statically significant.

## 3. Results

### 3.1. Patient cohort

Between January 2021 and December 2022, 102 patients (mean age 69 years ± 13 years 70 men) were included. 58 out of 102 patients presented with cerebral vessel occlusion as defined by corresponding abnormalities observed in VPCT. Patients' characteristics are presented in Table 1.

### 3.2. Quantitative evaluation

Compared to c-CTA, DLe-CTA demonstrated significantly superior results across various parameters in the quantitative evaluation of the BA, MCA, and SV per patient (all items $p < 0.001$). DLe-CTA demonstrated a significant increase in SNR (from c-CTA = 37.8 ± 14.6 to DLe-CTA = 108.5 ± 40.4; $p < 0.001$), CNR (from c-CTA = 32.0 ± 13.7 to DLe-CTA = 104.5 ± 39.7; $p < 0.001$) and slope (from c-CTA = 177.7 ± 50.7 to DLe-CTA = 406.1 ± 124.1; $p < 0.001$). The results of the various vessel sections are shown using box plots in Fig. 2.

**Table 2**
Comparison of the odds ratios of the various parameters.

| Parameter | OR | CI | p |
|---|---|---|---|
| **Overall Image Quality** | 3.23 | [2;8] | <0.001 |
| **Vessel Contrast** | 9.05 | [4;21] | <0.001 |
| **Artifacts** | 1.99 | [0;52] | 0.509 |
| **Diagnostic Confidence** | 2.56 | [1;7] | 0.029 |
| **Image Noise** | 0.61 | [0;2] | 0.460 |
| **Assessability of Proximal Vessels** | 2.64 | [1;7] | 0.023 |
| **Assessability of Intermediate Vessels** | 7.63 | [4;14] | <0.001 |
| **Assessessability of Subcortical Vessels** | 5.98 | [4;9] | <0.001 |

Note.—OR = odds ratio. CI = confidence interval. p = p-value.

HU measurement within the proximal middle cerebral artery mirrored this observation with a mean vessel contrast for DLe-CTA of 481HU ± 140 HU vs. 229HU ± 63HU in c-CTA ($p < 0.001$).

### 3.3. Qualitative evaluation

DLe-CTA provided significantly higher scores for all defined parameters ($p < 0.05$) except for image noise and artifacts. Overall image quality (OR [95 % CI]: 3.23 [2;8], $p < 0.001$), vessel contrast (OR [95 % CI]: 9.05 [4;21], $p < 0.001$), diagnostic confidence (OR [95 % CI]: 2.56 [1;7]; $p < 0.05$) and the assessability of proximal (OR [95 % CI]: 2.64 [1;7]; $p < 0.05$), intermediate (OR [95 % CI]: 7.63 [4;14]; $p < 0.001$)

**Table 3**
Results of the interrater agreement.

| | Fleiss' Kappa c-CTA | Fleiss' Kappa DLe-CTA |
|---|---|---|
| **Overall Image Quality** | 0.66 | 0.64 |
| **Vessel Contrast** | 0.68 | 0.71 |
| **Artifacts** | 0.67 | 0.44 |
| **Diagnostic Confidence** | 0.75 | 0.71 |
| **Image Noise** | 0.66 | 0.61 |
| **Assessability of Proximal Vessels** | 0.63 | 0.81 |
| **Assessability of Intermediate Vessels** | 0.74 | 0.77 |
| **Assessability of Subcortical Vessels** | 0.69 | 0.80 |

Note.—c-CTA = conventional CTA. DLe-CTA = Deep Learning-enhanced CTA.

and subcortical (OR [95 % CI]: 5.98 [4;9]; $p < 0.001$) vessels were superior with DLe-CTA.

Table S2 provides an overview of the individual results of the three readers. Fig. 3 shows the distribution of the image quality scores. OR for all defined parameters are presented in Table 2.

For vessel contrast, the best possible score of 4 (homogeneous contrast throughout all vessel sections) was given in 40.2 % of DLe-CTAs compared to 1 % in c-CTAs ($p < 0.001$).

Interrater agreement ranged between moderate and almost perfect (Table 3).

### 3.4. Diagnostic accuracy analyses

Compared to c-CTA, DLe-CTA significantly increased sensitivity among readers ($p < 0.05$), particularly for DMVO. Readers 2 and 3 both correctly identified 48/58 patients of cerebral vessel occlusion (83 %; 95 % CI: 70.6 %-91.4 %) with c-CTA, compared to 55/58 patients (95 %; 95 % CI: 85.6 %-98.9 %) with DLe-CTA. Similarly, Reader 1′s sensitivity increased from 46/58 patients (79 %; 95 % CI: 66.7 %-88.8 %) with c-CTA to 53/58 patients (91 %; 95 % CI: 81.0 %-97.1 %) with DLe-CTA.

The subgroup analysis showed no significant differences for DLe-CTA compared to c-CTA in PLVO (all readers 100 %, 95 % CI: 86.8 %-100 %) and MeVO. While readers 2 and 3 showed perfect sensitivity for DLe-CTA and c-CTA in MeVO (100 %, 95 % CI: 86.8 %-100 %), reader 1 correctly recognised 12/13 in c-CTA (92 %, 95 % CI: 64.0 %-99.8 %) and 13/13 in DLe-CTA (100 %, 95 % CI: 86.8 %-100 %). In DMVO, sensitivity increased significantly in all readers (readers 1–3: $p < 0.05$). Reader 1 recognised 8/19 occlusions in the c-CTA (42 %, 95 % CI: 20.3 %-66.5 %) versus 14/19 in the DLe-CTA (73 %, 95 % CI: 40.1 %-91.3 %). Reader 2 and 3 performed slightly better with 9/19 in the c-CTA (47, 95 % CI: 24.4 %-71.1 %) versus 16/19 in the DLe-CTA (84 %, 95 % CI: 60.4 % versus 96.6 %).

In summary, DLe-CTA is significantly superior to c-CTA in the detection of DMVO. In contrast, there are no significant differences in the detection of PLVO and MeVO.

Readers 2 and 3 had no false positive findings (specificity: 100 %; 95 % CI: 92.0 %-100 %). On the other hand, Reader 1 had one false positive finding in DLe-CTA, resulting in a specificity of 43/44 (98 %; 95 % CI: 88.0 %-99.9 %).

Table 4 summarizes the readers' sensitivity and specificity.

Figs. 4 and 5 illustrate examples of c-CTA and DLe-CTA of patients with suspected stroke, in which readers could detect vessel occlusions using DLe-CTA but not in the c-CTA images. Fig. 6 shows the false positive finding on DLe-CTA produced by Reader 1.

## 4. Discussion

This study investigates the effects of a deep leaning-based algorithm for detecting and selectively enhancing iodinated contrast agents in single-energy images on overall image quality and the sensitivity and

**Table 4**
Sensitivity and specificity for detecting cerebral vessel occlusions.

| | c-CTA | | | | | | | | | | | | DLe-CTA | | | | | | | | | | | |
|---|---|---|---|---|---|---|---|---|---|---|---|---|---|---|---|---|---|---|---|---|---|---|---|---|
| | Reader 1 | | | | Reader 2 | | | | Reader 3 | | | | Reader 1 | | | | Reader 2 | | | | Reader 3 | | | |
| | all | PLVO | MeVO | DMVO | all | PLVO | MeVO | DMVO | all | PLVO | MeVO | DMVO | all | PLVO | MeVO | DMVO | all | PLVO | MeVO | DMVO | all | PLVO | MeVO | DMVO |
| **True positive** | 46 | 26 | 12 | 8 | 48 | 26 | 13 | 9 | 48 | 26 | 13 | 9 | 53 | 26 | 13 | 14 | 55 | 26 | 13 | 16 | 55 | 26 | 13 | 16 |
| **False negative** | 12 | 0 | 1 | 11 | 10 | 0 | 0 | 10 | 10 | 0 | 0 | 10 | 5 | 0 | 0 | 5 | 3 | 0 | 0 | 3 | 3 | 0 | 0 | 3 |
| **True negative** | 44 | | | | 44 | | | | 44 | | | | 44 | | | | 43 | | | | 44 | | | |
| **False positive** | 0 | | | | 0 | | | | 0 | | | | 0 | | | | 1 | | | | 0 | | | |
| **Sensitivity [in %]** | | 100 | 92 | 42 | | 100 | 100 | 47 | | 100 | 100 | 47 | | 100 | 100 | 73 | | 100 | 100 | 84 | | 100 | 100 | 84 |
| | 79 (67–89) | | | | 83 (71–91) | | | | 83 (71–91) | | | | 91 (81–97) | | | | 95 (86–99) | | | | 95 (86–99) | | | |
| **Specificity [in %]** | 100 (92–100) | | | | 100 (92–100) | | | | 100 (92–100) | | | | 98 (88–100) | | | | 100 (92–100) | | | | 100 (92–100) | | | |

Note.—Data in parentheses are 95 % confidence intervals. c-CTA = conventional CTA. DLe-CTA = Deep Learning-enhanced CTA. PLVO = proximal large vessel occlusions. MeVO = medium vessel occlusions. DMVO = distal, medium vessel occlusions.

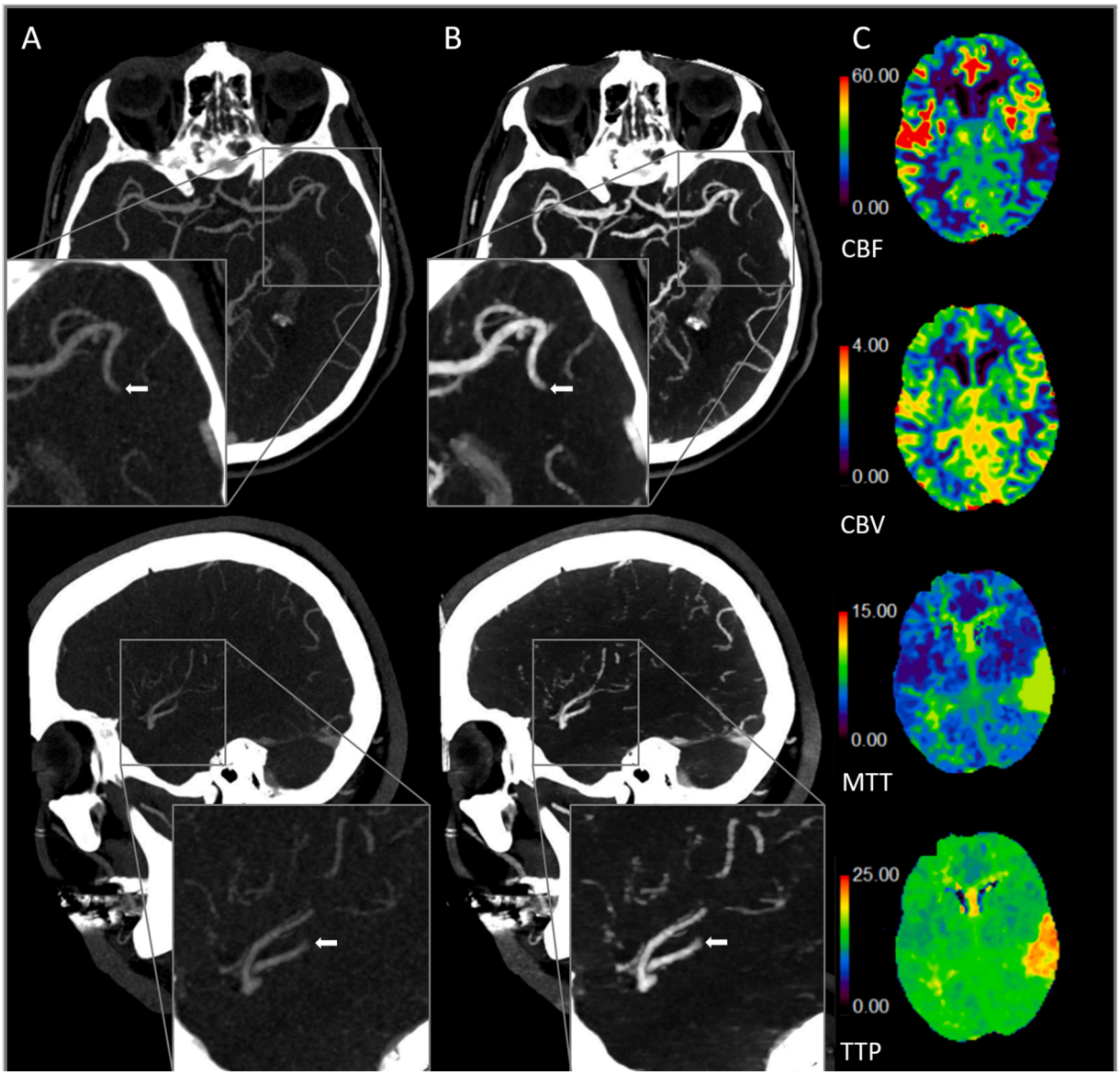


**Fig. 4.** Comparison of c-CTA (A) and DLe-CTA (B) with VPCT as a reference standard in a 65-year-old male patient with M2 occlusion on the left side (arrows) and a suitable correlate in the VPCT (C). Two of the three readers only detected the vessel occlusion in the DLe-CTA. c-CTA = conventional CTA. DLe-CTA = Deep Learning-enhanced CTA. CBF = cerebral blood low. CBV = cerebral blood volume. MTT = mean transit time. TTP = time to peak.

specificity for detecting cerebral vessel occlusions in patients with suspected stroke. Our analyses demonstrated that DLe-CTA achieved significantly superior values for SNR and CNR, as well as notable increase in contrast intensity and slope compared to c-CTA in the quantitative evaluation. These findings were corroborated by the objective assessment, which revealed significantly higher values for all defined parameters, including overall image quality, vessel contrast, diagnostic confidence and assessability of various vessel segments. The analysis of sensitivity and specificity in the detection of vascular occlusions ultimately showed a significant increase in the detection of DMVO, while no significant differences were found in the detection of PLVO and MeVO.

Dual-energy CT and photon-counting CT, as well as virtual monoenergetic imaging reconstruction, is an active area of research in various organ systems [3,12–14]. Virtual monoenergetic imaging reconstructions utilise the different energy levels of dual-energy CT to generate images at specific virtual energies, enhancing tissue differentiation and improving the vascularization of vascular structures [15]. They have been shown to improve image quality and contrast in various body regions [16–21]. Weiss et al. investigated the impact of sensitivity enhancement using virtual monoenergetic imaging reconstruction. The authors found virtual monoenergetic imaging reconstruction to significantly increase vessel contrast at low energy levels, allowing for better morphological assessment of pulmonary in detecting incidental pulmonary embolism in oncology patients [22].

Artificial intelligence makes it possible to create algorithms through deep learning that learn/imitate these properties and possibilities of spectral imaging in parts. These can then be used independently of the device through secondary image processing.

To our knowledge, our study is the first to evaluate the effects of deep learning-enhanced iodine contrast on image quality and diagnostic accuracy of CTA in stroke patients. In addition to denoising, the deep learning-based algorithm in this study is trained with dual-energy CT data and can detect iodine and selectively enhance it in single-energy data (ClariACE, ClariPi) [23–25]. To better understand the effect of deep learning-enhanced contrast intensity on stroke imaging, we selected CTAs with poor contrast to detect potential advantages of this. The increase in sensitivity of DMVO for the CTAs we defined as poorly contrasted is a remarkable result. Especially in the context of the

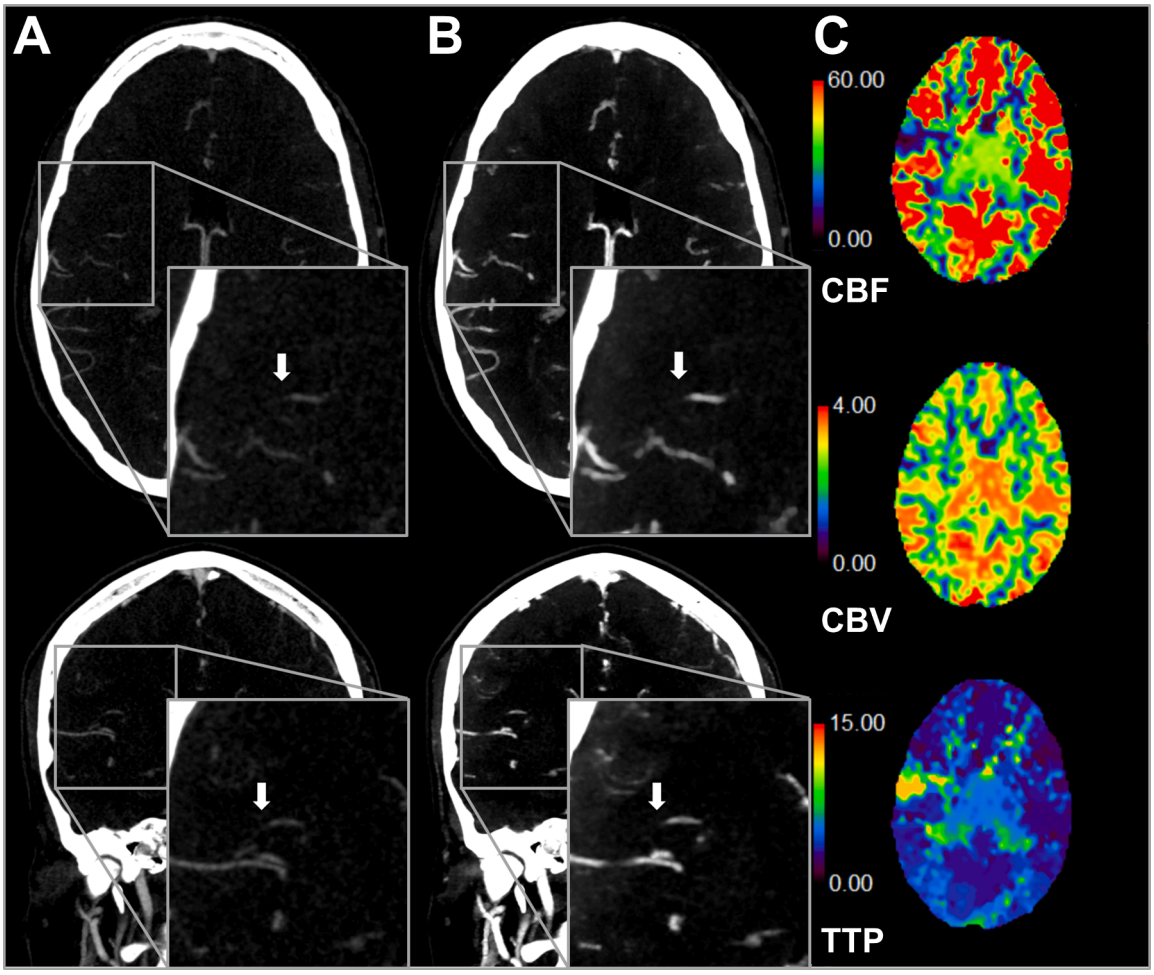


**Fig. 5.** Comparison of c-CTA (A) and DLe-CTA (B) with VPCT as reference standard in a 37-year-old male patient with M3 occlusion on the right side and a suitable correlate in the VPCT (C) with compensated CBV. This closure was recognized by all three readers exclusively in the DLe-CTA. c-CTA = conventional CTA. DLe-CTA = Deep Learning-enhanced CTA. CBF = cerebral blood low. CBV = cerebral blood volume. MTT = mean transit time.

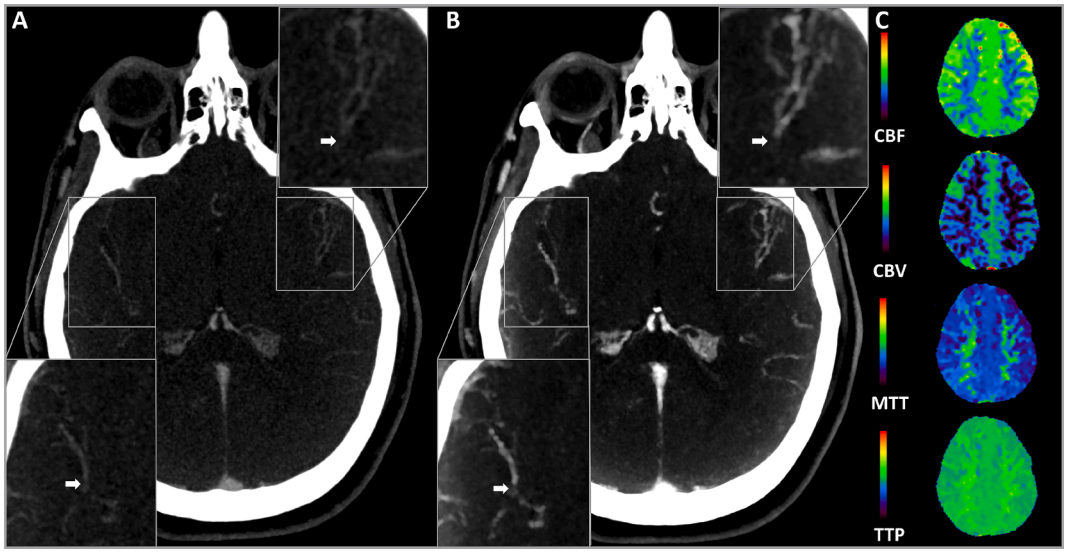


**Fig. 6.** This figure compares the false positive finding of Reader 2 in DLe-CTA (B) with c-CTA (A). In the enlargements, the false positive finding is marked on the right and a similar "finding" is marked on the opposite side for clarification. Symmetrical visualization of VPCT (C) without evidence of cerebral vessel occlusion. c-CTA = conventional CTA. DLe-CTA = Deep Learning-enhanced CTA. CBF = cerebral blood low. CBV = cerebral blood volume. MTT = mean transit time. TTP = time to peak.

increasing importance of mechanical thrombectomy of such occlusions, algorithms such as the one analysed here could contribute to an improvement in the treatment of stroke patients [26–28].

An interesting point would be the combination of different AI algorithms and metaheuristic optimization techniques, such as the Prairie Dog Optimisation Algorithm and the Dwarf Mongoose Optimisation Algorithm [29,30]. There is already scientific evidence that hybrid approaches, which combine multiple metaheuristic strategies, perform better than one approach alone, as they utilise the respective strengths more efficiently and compensate for the weaknesses [31,32]. Future studies should analyse how algorithms at different levels of processing interact with each other and how their positive effects and weaknesses affect each other.

This study has limitations. The retrospective study design may have led to selection bias. Another point is that the small sample size could lead to a lower power. Both aspects may limit the generalizability of the results. Furthermore, this study analyzed data from a single center on a single scanner, but the deep learning model is vendor diagnostic. Therefore, further research, such as prospective studies or trials involving multiple centers, is needed to validate and generalize our findings. They should include all patients with suspected stroke to investigate to what extent the positive results of using vendor diagnostic advantages of spectral imaging observed in this study can be generalized under everyday examination conditions. Another limitation must be discussed in the VPCT used as a gold standard. The VPCT is very susceptibility prone for movement artifacts and application problems of the contrast medium. Further, some ischemic areas, such as lacunary defects, are challenging to detect.

## 5. Conclusion

We found Deep-learning enhanced contrast and noise reduction to improve the diagnostic accuracy of DMVO in poorly contrasted CTA, potentially contributing to better treatment of patients with acute stroke, especially in the context of the increasing importance of mechanical thrombectomy for distal vascular occlusions.

This research did not receive any specific grant from funding agencies in the public, commercial, or not-for-profit sectors.

During the preparation of this work the author used Grammarly.com in order to improve grammar and readability. After using this tool/service, the author reviewed and edited the content as needed and takes full responsibility for the content of the published article.

## CRediT authorship contribution statement

**Sebastian Steinmetz:** Writing – review & editing, Writing – original draft, Visualization, Resources, Project administration, Methodology, Investigation, Formal analysis, Data curation, Conceptualization. **Mario Alberto Abello Mercado:** Investigation, Formal analysis. **Sebastian Altmann:** Writing – review & editing, Writing – original draft, Visualization, Resources, Project administration, Methodology, Investigation, Formal analysis, Data curation, Conceptualization. **Antoine Sanner:** Validation, Software, Formal analysis. **Andrea Kronfeld:** Software, Formal analysis, Conceptualization. **Marius Frenzel:** Writing – review & editing. **Dongok Kim:** Software. **Sergiu Groppa:** Supervision, Data curation. **Timo Uphaus:** Supervision, Data curation. **Marc A. Brockmann:** Writing – review & editing, Validation, Supervision, Project administration, Data curation, Conceptualization. **Ahmed E. Othman:** Writing – review & editing, Writing – original draft, Validation, Supervision, Resources, Project administration, Methodology, Investigation, Formal analysis, Data curation, Conceptualization.

## Declaration of competing interest

The authors declare that they have no known competing financial interests or personal relationships that could have appeared to influence the work reported in this paper.

## Appendix A. Supplementary data

Supplementary data to this article can be found online at https://doi.org/10.1016/j.ejrad.2024.111808.

## References

[1] S.S. Martin, A.W. Aday, Z.I. Almarzooq, et al., 2024 heart disease and stroke statistics: a report of US and global data from the american heart association, Circulation 149 (8) (2024) e347–e913.
[2] A.M. Mortimer, E. Simpson, M.D. Bradley, S.A. Renowden, Computed tomography angiography in hyperacute ischemic stroke: prognostic implications and role in decision-making, Stroke 44 (5) (2013) 1480–1488.
[3] T. D'Angelo, G. Cicero, S. Mazziotti, et al., Dual energy computed tomography virtual monoenergetic imaging: technique and clinical applications, Br J Radiol. 92 (1098) (2019) 20180546.
[4] D. Leithner, J.L. Wichmann, T.J. Vogl, et al., Virtual monoenergetic imaging and iodine perfusion maps improve diagnostic accuracy of dual-energy computed tomography pulmonary angiography with suboptimal contrast attenuation, Invest Radiol. 52 (11) (2017) 659–665.
[5] T. D'Angelo, A.M. Bucher, L. Lenga, et al., Optimisation of window settings for traditional and noise-optimised virtual monoenergetic imaging in dual-energy computed tomography pulmonary angiography, Eur Radiol. 28 (4) (2018) 1393–1401.
[6] H. Gong, J.F. Marsh, K.N. D'Souza, et al., Deep-learning-based direct synthesis of low-energy virtual monoenergetic images with multi-energy CT, J Med Imaging (bellingham). 8 (5) (2021) 052104.
[7] W. Cong, Y. Xi, P. Fitzgerald, B. De Man, G. Wang, Virtual monoenergetic CT imaging via deep learning, Patterns (n y). 1 (8) (2020) 100128.
[8] F.A. Ucar, M. Frenzel, A. Kronfeld, et al., Improvement of neurovascular imaging using ultra-high-resolution computed tomography angiography, Clin Neuroradiol. 34 (1) (2024) 189–199.
[9] R.G. Nogueira, M.F. Doheim, A.R. Al-Bayati, et al., Distal medium vessel occlusion strokes: understanding the present and paving the way for a better future, J Stroke. 26 (2) (2024) 190–202.
[10] J.L. Saver, R. Chapot, R. Agid, et al., Thrombectomy for distal, medium vessel occlusions: a consensus statement on present knowledge and promising directions, Stroke 51 (9) (2020) 2872–2884.
[11] W. Tang, J. Hu, H. Zhang, P. Wu, H. He, Kappa coefficient: a popular measure of rater agreement, Shanghai Arch Psychiatry. 27 (1) (2015) 62–67.
[12] D. Dillinger, D. Overhoff, C. Booz, et al., Impact of CT photon-counting virtual monoenergetic imaging on visualization of abdominal arterial vessels, Diagnostics (basel) 13 (5) (2023).
[13] T. Sartoretti, M. McDermott, V. Mergen, et al., Photon-counting detector coronary CT angiography: impact of virtual monoenergetic imaging and iterative reconstruction on image quality, Br J Radiol. 96 (1143) (2023) 20220466.
[14] A. Meloni, F. Cademartiri, L. Pistoia, et al., Dual-source photon-counting computed tomography-part iii: clinical overview of vascular applications beyond cardiac and neuro imaging, J Clin Med. 12 (11) (2023).
[15] Y. Zeng, D. Geng, J. Zhang, Noise-optimized virtual monoenergetic imaging technology of the third-generation dual-source computed tomography and its clinical applications, Quant Imaging Med Surg. 11 (11) (2021) 4627–4643.
[16] C.N. De Cecco, D. Caruso, U.J. Schoepf, et al., A noise-optimized virtual monoenergetic reconstruction algorithm improves the diagnostic accuracy of late hepatic arterial phase dual-energy CT for the detection of hypervascular liver lesions, Eur Radiol. 28 (8) (2018) 3393–3404.
[17] J.X. Li, F.J. Xie, C.H. Chen, K.M. Chen, C.J. Tsai, Dual-energy computed tomography for evaluation of breast cancer follow-ups: comparison of virtual monoenergetic images and iodine-map, Diagnostics (basel) 12 (4) (2022).
[18] L. Lenga, M.H. Albrecht, A.E. Othman, et al., Monoenergetic dual-energy computed tomographic imaging: cardiothoracic applications, J Thorac Imaging. 32 (3) (2017) 151–158.
[19] M. Kaup, J.E. Scholtz, A. Engler, et al., Dual-energy computed tomography virtual monoenergetic imaging of lung cancer: assessment of optimal energy levels, J Comput Assist Tomogr. 40 (1) (2016) 80–85.
[20] J.E. Scholtz, J.L. Wichmann, D.W. Bennett, et al., Detecting intracranial hemorrhage using automatic tube current modulation with advanced modeled iterative reconstruction in unenhanced head single- and dual-energy dual-source CT, AJR Am J Roentgenol. 208 (5) (2017) 1089–1096.
[21] C.T. Arendt, R. Czwikla, L. Lenga, et al., Improved coronary artery contrast enhancement using noise-optimised virtual monoenergetic imaging from dual-source dual-energy computed tomography, Eur J Radiol. 122 (2020) 108666.
[22] J. Weiss, M. Notohamiprodjo, M. Bongers, et al., Effect of noise-optimized monoenergetic postprocessing on diagnostic accuracy for detecting incidental pulmonary embolism in portal-venous phase dual-energy computed tomography, Invest Radiol. 52 (3) (2017) 142–147.
[23] T. Lee, J.M. Lee, J.H. Yoon, et al., Deep learning–based image reconstruction of 40-keV virtual monoenergetic images of dual-energy CT for the assessment of hypoenhancing hepatic metastasis, Eur. Radiol. 32 (9) (2022) 6407–6417.

[24] S. Park, J.H. Yoon, I. Joo, et al., Image quality in liver CT: low-dose deep learning vs standard-dose model-based iterative reconstructions, Eur. Radiol. 32 (5) (2022) 2865–2874.
[25] T. Lee, J.H. Yoon, J.Y. Park, et al., Deep learning-based iodine contrast-augmenting algorithm for low-contrast-dose liver CT to assess hypovascular hepatic metastasis, Abdominal Radiology. 48 (11) (2023) 3430–3440.
[26] S. Matsoukas, S.G. Paz, C.P. Kellner, et al., Endovascular thrombectomy for distal vessel occlusion stroke: Single-center experience, Interv Neuroradiol. (2023).
[27] D. Sepp, M.R. Hernandez Petzsche, T. Zarth, et al., Mechanical thrombectomy of distal cerebral vessel occlusions of the anterior circulation, Sci Rep. 13 (1) (2023) 5730.
[28] L. Meyer, C.P. Stracke, M. Wallocha, et al., Thrombectomy for secondary distal, medium vessel occlusions of the posterior circulation: seeking complete reperfusion, J Neurointerv Surg. 14 (7) (2022) 654–659.
[29] M. Hijjawi, M. Alshinwan, O.A. Khashan, et al., A novel hybrid prairie dog algorithm and harris hawks algorithm for resource allocation of wireless networks, IEEE Access 11 (2023) 145146–145166.
[30] O. Akinola, J.O. Agushaka, A.E. Ezugwu, Binary dwarf mongoose optimizer for solving high-dimensional feature selection problems, PLoS One 17 (10) (2022) e0274850.
[31] E. Eker, M. Kayri, S. Ekinci, D. İzci, Comparison of swarm-based metaheuristic and gradient descent-based algorithms in artificial neural network training, Adcaij Advances in Distributed Computing and Artificial Intelligence Journal. 12 (1) (2023) e29969.
[32] E.-S.-M. El-kenawy, A.A. Abdelhamid, A. Ibrahim, et al., Al-Biruni Earth Radius (BER) metaheuristic search optimization algorithm, Comput. Syst. Sci. Eng. 45 (2) (2023) 1917–1934.